doi:10. 3772/j. issn. 1006-6748. 2023. 02. 005

Research on the dynamic response of connecting rod bearing bush wear of reciprocating machine under variable working conditions①

ZHANG Jinjie(张进杰)*, SONG Chunyu*, LEI Fuchang*, WANG Yao②*,
ZHI Haifeng**, LIU Fengchun**
(*Beijing Key Laboratory of Health Monitoring and Self-Healing of High-end Mechanical Equipment, Beijing University of Chemical Technology, Beijing 100029, P. R. China)
(**China North Engine Research Institute (Tianjin), Tianjin 300400, P. R. China)

Abstract

As a type of reciprocating machine, the reciprocating compressor has a compact structure and many excitation sources. Once the small end bearing of the connecting rod is worn, it is easy to cause the sintering of the bearing and the abnormal vibration of the body. Based on the characteristics of poor lubrication state and complex force of connecting rod small head bearing, a mixed lubrication model considering oil groove feed was established, and the dynamic simulation of the reciprocating compressor model with lubricated bearings was carried out; considering different speeds and gas load conditions, the law of the impact of the eigenvalues changing with working conditions was explored. The fault simulation experiment was carried out by selecting representative working conditions, which verified the correctness of the simulation method. The study found that two contact collisions between the pin and the bearing bush occurred in one cycle, the collision impact was more severe under the wear fault, and the existence of the gap made the dynamic response more sensitive to the change of working conditions. This research provides ideas for the location and feature extraction of fault symptom signal angular segments in the process of complex measured signal processing.

Key words: small head tile, wear, lubrication, variable working condition, impact

0 Introduction

Reciprocating compressor connecting rod small head bearings are at the end of the lubrication system and operate at low speed, with complex forces and poor lubrication status, and the surfaces of mating parts often produce direct contact and work in a mixed lubrication state[1-2]. Many scholars describe the bearing forces under different motion states by establishing hybrid models when constructing lubrication models. Ref. [3] proposed a hybrid model for gap joints, including three sub-models types: lubrication, transition force, and contact collision. Ref. [4] considered the characteristics of material surface elastic deformation when the eccentricity is large, and established a hybrid model with coupled dynamic lubrication model and elastohydrodynamic lubrication model. However, these hybrid models separate different motion states and ignore the simultaneous existence of contact and lubrication on the part surface in the hybrid lubrication state. Ref. [5] established the average Reynolds equation, which considers the effect of rough peaks on fluid lubrication and is suitable for calculating the oil film pressure in hybrid lubrication. Ref. [6] proposed a method for calculating the rough contact pressure in hybrid lubrication. The combination of these two types of models can find the surface pressure distribution under mixed lubrication.

The main research method currently used to analyze mechanism dynamics and bearing lubrication characteristics is jointly solving the lubrication model of a bearing and the dynamics equations of a mechanical mechanism. Refs [7, 8] coupled the lubrication model of a bearing containing clearance with a multi-body dynamics model and applied it to the bearings at the large and small ends of a connecting rod in a piston-connection-rod-crank system of a four-stroke engine. Ref. [9] developed a hybrid model containing dynamic lubrication, microscopic viscoelastic hydrodynamic lubrication

① Supported by the National Natural Science Foundation of China (No. 52101343).
② To whom correspondence should be addressed. E-mail: wyaobeijing@163. com.
Received on June 2, 2022

and Hertzian contact, and applied it to the dynamics analysis of engine connecting rod big-end bearings. Ref. [10] referred to the hybrid model in Ref. [3] and conducted a study on the dynamic response and nonlinear characteristics of a complex mechanism of multiple connecting rods containing multiple lubrication gap joints, and found that an increase in the gap value and speed diminishes the stability of the structure. Refs [11, 12] analyzed the time and spectral response of plain bearings in rotating machines under different wear profiles and found that wear increased the anisotropy of the system and led to a significant increase in the backward harmonic component (-1x) in the full spectral response.

In the research on the dynamics of reciprocating compressors with clearance motion pairs, few studies consider the effect of lubrication on rotating motion pairs. Refs [13 -15] applied a collision model at the clearance, ignoring lubrication effect. Therefore, this study analyzes the lubrication performance and dynamic response of the compressor transmission mechanism with lubrication gap under different speeds and gas loads, to provide a theoretical reference for the wear fault monitoring of the small head tile of the reciprocating compressor.

1 Mathematical model

1.1 Hybrid lubrication model

The average Reynolds equation proposed by Patir and Cheng in Ref. [5], which describes the effect of randomly distributed rough peaks on dynamic lubrication, is used in the fluid lubrication area:

$$\frac{\partial}{\partial x}\left(\varphi_x \frac{h^3}{12\mu}\frac{\partial \bar{P}}{\partial x}\right)+\frac{\partial}{\partial z}\left(\varphi_z \frac{h^3}{12\mu}\frac{\partial \bar{P}}{\partial y}\right)=\frac{U_1+U_2}{2}\frac{\partial \bar{h}_T}{\partial x}+\frac{U_1-U_2}{2}\sigma\frac{\partial \varphi_S}{\partial x}+\frac{\partial \bar{h}_T}{\partial t} \quad (1)$$

where, U_1 and U_2 are the journal and bearing surface travel velocities, respectively; φ_x and φ_z are the pressure flow factor; φ_S is the shear flow factor; h is the oil film thickness taking into account the total deformation; $\bar{h}_T$ is the average oil film thickness; σ is the combined standard deviation of roughness; $\bar{P}$ is the average oil film pressure; and μ is the lubricating oil viscosity. The directions of x and y are shown in Fig. 1(a), and the direction of z is the axial direction of the pin.

In the surface rough contact area, the rough surface contact model proposed by Greenwood and Tripp in Ref. [6] was used to calculate the rough contact pressure as

$$\bar{P}_C=\frac{16\sqrt{2}}{15}\pi(\lambda\chi\sigma)^2E\sqrt{\frac{\sigma}{\chi}}F_{2.5}(H) \quad (2)$$

where, λ is the peak element density of the rough surface, χ is the radius of curvature of the peak element, and E is the integrated modulus of elasticity. Determine whether rough surface contact has occurred by determining the magnitude of the film thickness ratio H:

$$F_{2.5}(H)=\begin{cases}4.4086\times10^{-5}(4-H)^{6.804} & H\leqslant 4\\ 0 & H>4\end{cases} \quad (3)$$

The surface of mixed lubrication is composed of fluid lubrication area and surface rough contact area, and the external load is borne by the corresponding oil film pressure and contact pressure. According to Fig. 1(a), the component forces of the bearing reaction force in the x and y directions can be expressed as

$$F_x=\sin\gamma\iint_\Omega(\bar{P}+\bar{P}_c)\cos\theta\mathrm{d}x\mathrm{d}y+\cos\gamma\iint_\Omega(\bar{P}+\bar{P}_c)\sin\theta\mathrm{d}x\mathrm{d}y \quad (4)$$

$$F_y=\cos\gamma\iint_\Omega(\bar{P}+\bar{P}_c)\cos\theta\mathrm{d}x\mathrm{d}y-\sin\gamma\iint_\Omega(\bar{P}+\bar{P}_c)\sin\theta\mathrm{d}x\mathrm{d}y \quad (5)$$

where Ω represents the entire lubrication domain.

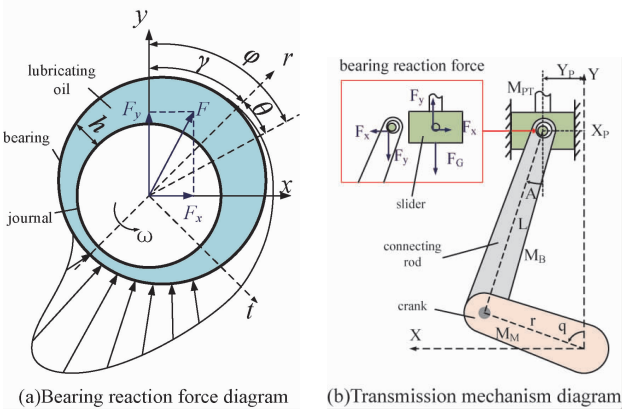

(a)Bearing reaction force diagram (b)Transmission mechanism diagram

Fig. 1 Diagram of transmission mechanism with lubrication gap

1.2 Multi-body dynamics model

Fig. 1(b) shows the schematic diagram of the drive mechanism, which can be divided into two parts: the crank linkage and the slider assembly. Ref. [16] established the dynamic equations of the crank linkage subsystem by the second form of the Lagrangian method. The equation of motion of the slider assembly can be expressed as

$$M_{\mathrm{PT}}\cdot\ddot{\boldsymbol{X}}_{\mathbf{PT}}=-\boldsymbol{F}_G-\boldsymbol{F}_y-(\boldsymbol{M}_{PT}\cdot g) \quad (6)$$

where, $\boldsymbol{F}_G$ is the combined force of the gas forces in the cylinder, $\ddot{\boldsymbol{X}}_{\mathbf{PT}}$ is the acceleration of the slider assembly, $\boldsymbol{M}_{\mathrm{PT}}$ is the mass of the slider assembly, and g

is the acceleration of gravity.

There are four thermodynamic processes in the operation of reciprocating compressors, which are expansion, inhalation, compression and exhaust, and the real-time pressure change in the cylinder can be obtained by establishing the cylinder thermodynamic differential equation[17].

Expansion process:

$$p_{cy}V_{cy}^{m_e}=p_{exp}V_{cle}^{m_e} \tag{7}$$

where, p_{cy} is the cylinder air pressure, V_{cy} is the cylinder gas volume, p_{exp} is the residual gas pressure, V_{cle} is the residual volume, m_e is the expansion process index.

Inhalation process:

$$\frac{\mathrm{d}p_{cy}}{\mathrm{d}t}=-\frac{\kappa p_{cy}}{V_{cy}}\frac{\mathrm{d}V_{cy}}{\mathrm{d}t}+\kappa p_s\frac{\alpha_{dv}A_{dv}}{V_{cy}}\sqrt{\frac{2\kappa R T_s}{\kappa-1}\left(\frac{p_{cy}}{p_s}\right)^{\frac{2}{\kappa}}\left[1-\left(\frac{p_{cy}}{p_s}\right)^{\frac{\kappa-1}{\kappa}}\right]} \tag{8}$$

where, p_s is the suction pressure, $\alpha_{dv}A_{dv}$ is the equivalent flow area of the valve, R is the thermal gas constant, and T_s is the temperature of the gas in the suction valve.

Compression process:

$$p_{cy}V_{cy}^{m_c}=p_sV_s^{m_c} \tag{9}$$

where, V_s is the volume of the inhaled gas and m_c is the compression process index.

Exhaust process:

$$\frac{\mathrm{d}p_{cy}}{\mathrm{d}t}=\frac{\kappa}{V_{cy}}\left\{p_{cy}\frac{\mathrm{d}V_{cy}}{\mathrm{d}t}+p_{cy}\alpha_{dv}A_{dv}\sqrt{\frac{2\kappa R T_d}{\kappa-1}\left(\frac{p_d}{p_{cy}}\right)^{\frac{2}{\kappa}}\left[\left(\frac{p_{cy}}{p_d}\right)^{\frac{\kappa-1}{\kappa}}-1\right]}\right\} \tag{10}$$

where, p_d is the exhaust pressure, and T_d is the gas temperature in the exhaust cylinder. The gas force F_G can be obtained through the real-time gas pressure of the above four processes.

In addition to the gas force F_G, the acting force at the crankshaft connecting rod also includes the reciprocating inertial force F_I and the friction force F_f. The friction force value is much smaller than the above two forces and can be ignored. The reciprocating inertial force can be expressed as

$$\boldsymbol{F_I}=M_{rec}\cdot\boldsymbol{a}=(M_{PT}+0.3M_B)\cdot r\dot{\boldsymbol{q}}^2\left(\cos\boldsymbol{q}+\frac{r}{L}\cos 2\boldsymbol{q}\right) \tag{11}$$

where, M_{rec} is the reciprocating mass, M_{PT} is the piston mass, M_B is the connecting rod mass, r is the crank length, L is the connecting rod length, $\dot{\boldsymbol{q}}$ is the crank angular velocity, and $\boldsymbol{a}$ is the reciprocating acceleration.

The sum of the axial forces of the connecting rod bearing is called the comprehensive piston force $\boldsymbol{F_p}$ (represented as $\boldsymbol{F_y}$ in Fig. 1), namely:

$$\boldsymbol{F_p}=\boldsymbol{F_I}+\boldsymbol{F_G}+\boldsymbol{F_f} \tag{12}$$

2 Simulation model establishment

Fig. 2 shows the horizontal opposed double-cylinder reciprocating compressor test bench, and its structure and operating parameters are shown in Table 1. Based on this experimental bench, a corresponding simulation model is established in SolidWorks, as shown in Fig. 3(a). Import the model into the multi-body dynamics software RecurDyn and apply loads and constraints to establish a multi-body dynamics model.

Fig. 2 Compressor fault simulation test bench

Table 1 Main parameters of the reciprocating compressor unit

Parameter Name	Value	Parameter Name	Value
Crank length (r)	90 mm	Bearing inner diameter (R_j)	50 mm
Connecting rod length (L)	450 mm	Bearing width (B)	120 mm
Slider assembly quality(M_{PT})	48.2 kg	Bearing clearance (c)	0.1 mm
Crankshaft quality (M_M)	72 kg	Viscosity oflubricating oil (μ)	2e-2 Pa·s
Connecting rod quality (M_B)	14 kg	Integrated standard deviation of roughness (σ)	1e-3 mm
Exhaust pressure (p_d)	0.3 MPa	Integrated modulus of elasticity(E)	68 000 N/mm^2
Crankshaft speed	500 r/min	Oil groove feed pressure (p_h)	0.12 MPa

The crankshaft of the compressor is driven by the electric motor at a constant angular velocity such as 500 r/min. The load of the model is the gas force exerted on the piston, which is calculated by the mathematical model above. In this paper, the regulation method of opening the intake valve with partial stroke is used to achieve variable load. Fig. 4 shows the gas pressure under various loads and Table 2 shows the constraint relationship between components.

The exciting force generated at the small end

bearing of the connecting rod is transmitted to the mid-body slide through the crosshead. To further study the vibration response of the monitorable surface and improve the simulation accuracy, the components in the vibration transmission path (small head tile, crosshead pin, crosshead and mid-body slide) were modal flexible, as shown in Fig. 3(b). The mesh type is selected as tetrahedron, the mesh size of the crosshead midbody and crosshead is 20 mm, the mesh size of the connecting rod small end bushing and the crosshead pin is 10 mm, and the number of free modes is 10.

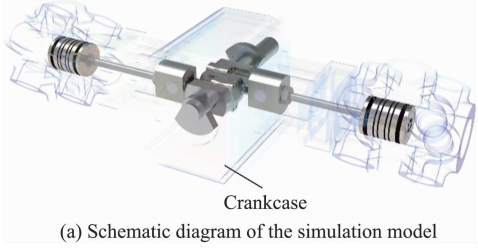

(a) Schematic diagram of the simulation model

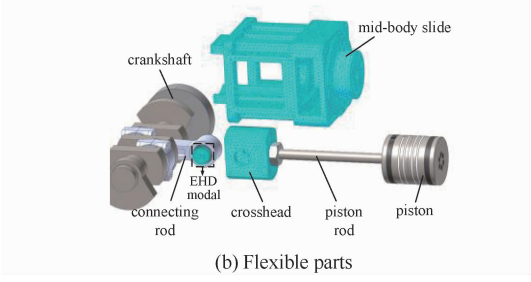

(b) Flexible parts

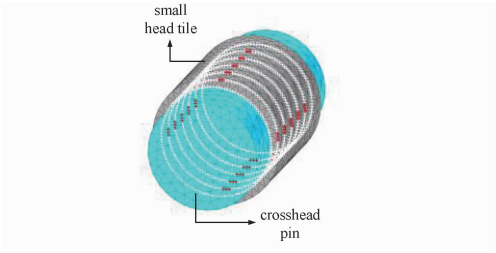

(c) EHD model

Fig. 3 Schematic diagram of the simulation model

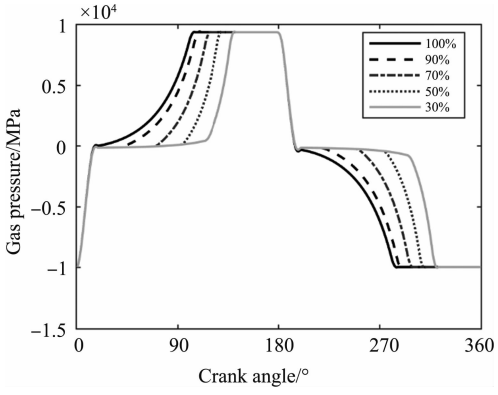

Fig. 4 Gas force under various loads

Table 2 The constraints between components

Components	Constraints
Ground and crankcase	Fixed
Crankcase and crankshaft	Revolution
Crankshaft pin and connecting rod big end	Revolution
Connecting rod small end and small head tile	Fixed
Small head tile and crosshead pin	EHD
Crosshead pin and crosshead	Fixed
Crosshead and mid-body slide	Translation
Crosshead and piston rod	Fixed
Piston rod and piston	Fixed

In the RecurDyn software, the tool Rotational Lubrication can establish the model of elastohydrodynamic lubrication (EHD), which couples the Reynolds equation and the rough surface contact model, and can describe the motion state of rough contact, complete lubrication and mixed lubrication. An EHD model is established between the small end tile and the crosshead pin of the modal flexible body connecting rod, as shown in Fig. 3(c). The key parameters are shown in Table 1. To introduce lubricating oil into the entire friction surface, oil holes or oil grooves must be opened on the bearing bush or journal, so the distribution of oil grooves and oil holes should be considered when analyzing the lubrication characteristics. The lubricating oil is supplied to the small end bearing of the connecting rod through the oil hole or oil groove of the small end bearing bush of the connecting rod after passing through the main bearing-the inner oil passage of the crankshaft-the large end bearing of the connecting rod-the inner oil passage of the connecting rod. The model is equipped with four axial oil grooves evenly distributed in the circumferential direction on the inner surface of the small head tile. The red mark in Fig. 3(c) indicates the grid points in the oil groove area, and the oil film pressure at the oil groove is the oil supply pressure.

3 Simulation and discussion

3.1 Experimental verification of simulation models

Analysis of the failure mechanism needs to involve a variety of variables and working conditions. However, it is difficult to conduct a large number of failure simulation experiments, and some characteristic values such as oil film characteristic parameters, axis trajectory and acceleration of moving parts are difficult to measure. Therefore, the simulation method is mainly used to carry out research. Select representative working conditions to carry out experiments to verify the correctness of the simulation model, and then carry out in-depth research through simulation methods. The crankshaft speed was set to 500 r/min and the gas load was 100%, and two sets of experiments were carried out

under normal conditions and under wear fault conditions. The fitting clearance at the small end bearing of the connecting rod of the compressor is 0.8% – 1.2% of the fitting diameter, and the standard clearance of this test bench is 0.1 mm; the wear is set to be evenly distributed in the circumferential direction of the bearing bush, and the wear clearance is 0.2 mm, which is in the early stage of wear failure.

By artificially manufacturing the inner surface of the bearing bush to wear, the fault injection to the small end bush of the connecting rod is realized. The wear part is processed on the inner surface of the small head tile by wire cutting technology to form a local wear profile, and the wear depth is 0.05 mm.

To measure the fault signal of the bearing bush impact at a closer distance, the acceleration sensor is installed on the upper surface of the mid-body slide on the side where the target small head bush is located. First, use the normal bearing bush, start running for 4 min, and use the data collector to collect data synchronously with the vibration sensor at the sampling frequency of 25.6 kHz; then stop and disassemble, replace the worn small head bush, and carry out the experiment under the same working conditions.

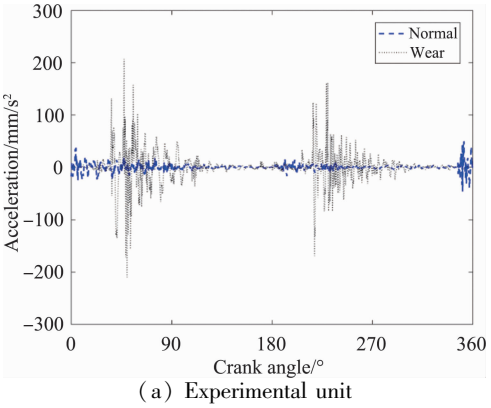

(a) Experimental unit

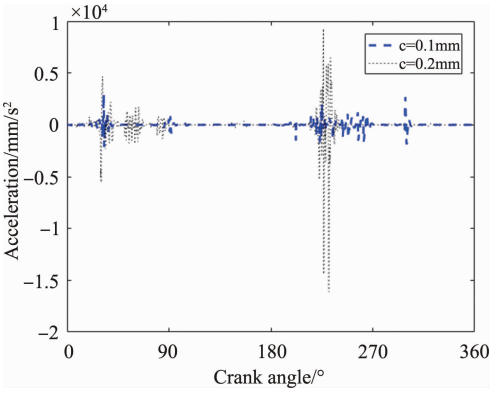

(b) Simulation model

Fig. 5 Comparison of experimental and simulated vibration acceleration

Fig. 5(a) is a comparison diagram of the vibration acceleration of the measuring point measured by the test bench under normal conditions and fault conditions. It can be seen that there are two shocks in one cycle under the two working conditions; under the wear condition, the shock amplitude is about four times that of the normal working condition, and the vibration shock is distributed at the crankshaft angle $q = 35 - 101°$ and $216 - 278°$, and the phase distribution range of the shock is larger than the normal working condition. Fig. 5(b) shows the vertical component of the vibration acceleration at the corresponding measurement point position in the simulation. It can be seen that there are two shocks in one cycle, and the shock phases are distributed in the crankshaft angle $q = 30 - 40°$ and $220 - 250°$; the impact amplitude of wear fault is about 4 – 5 times of normal working condition. The simulation results are consistent with the data law measured by the experimental unit, which can prove the correctness of the simulation model and further analyze other characteristic parameters in the simulation model.

Four clearance conditions of 0.1 mm, 0.15 mm, 0.2 mm and 0.25 mm were set in the simulation, and a series of dynamic responses are obtained, as shown in Fig. 6 – Fig. 10: bearing reaction forces $\boldsymbol{F}_x$, $\boldsymbol{F}_y$ in the horizontal and vertical directions; vibration accelerations Acx and Acy of crosshead in the horizontal and vertical direction; vibration accelerations Apx and Apy of the monitoring points on the surface of the mid-body slide in the horizontal and vertical direction; the motion trajectory of the center of mass of the crosshead pin relative to the small head tile; the schematic diagram of the surface pressure distribution.

Fig. 6 shows the comparison of bearing reaction force under four conditions: EHD model $c = 0.1$ mm, EHD model $c = 0.15$ mm, EHD model $c = 0.2$ mm and EHD model $c = 0.25$ mm. The force in the EHD model is obtained by integrating the oil film pressure and the contact pressure, corresponding to Eqs (1) – (5).

The EHD model has two relatively concentrated oscillations in one cycle. These oscillations originate from the impact between the pin and the bearing bush, and the impact generates the fault excitation force. The impact is mainly distributed in the crankshaft angle of $30 - 40°$ and $220 - 250°$. As the gap value increases, the amplitude of the oscillation increases significantly. The phase of the impact in the horizontal direction and the vertical direction is consistent, but the amplitude of the force oscilla-

tion in the horizontal direction is one order of magnitude larger than that in the vertical direction, that is, the impact motion mainly occurs in the horizontal direction.

Fig. 7 is the crosshead acceleration curves in the horizontal and vertical directions. It can be seen that in the phase of the shock in Fig. 6, the acceleration curve has corresponding oscillations in two directions, and the amplitude of the oscillation in the horizontal direction is one order of magnitude larger than that in the vertical direction. It can be seen that the crosshead at the same horizontal position as the fault excitation source retains the horizontal vibration to a large extent.

Fig. 8 shows the horizontal acceleration at the measuring point on the upper surface of the mid-body slide, and the curve oscillates at the impact phase. It can be seen that the acceleration oscillation amplitude in the vertical direction is 2 – 4 times that of the horizontal direction, which is inconsistent with the previous result that the horizontal component of the characteristic parameter is greater than the vertical component. This is because the constraint between the crosshead and the midbody slide is a sliding pair, and the contact surface normal is always perpendicular to the horizontal axis. Therefore, the vertical vibration is better preserved, while the main direction of vibration transmission-the horizontal vibration is lost a lot.

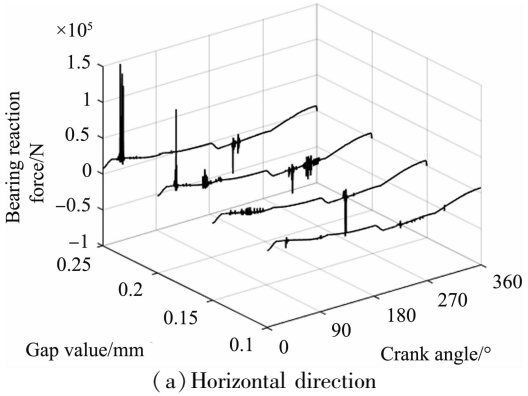

(a) Horizontal direction

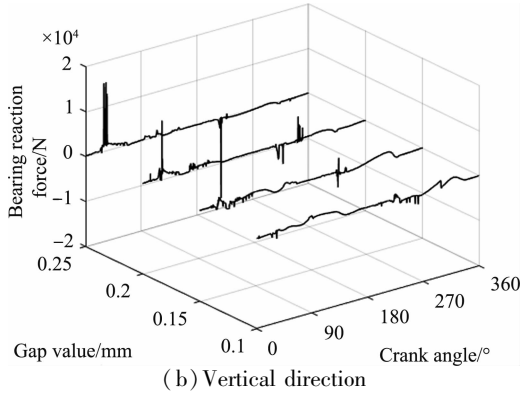

(b) Vertical direction

Fig. 6 Bearing reaction force of different models

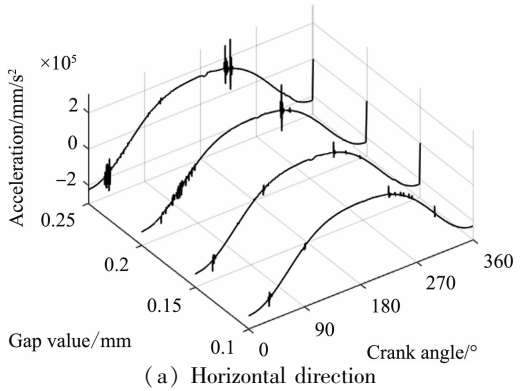

(a) Horizontal direction

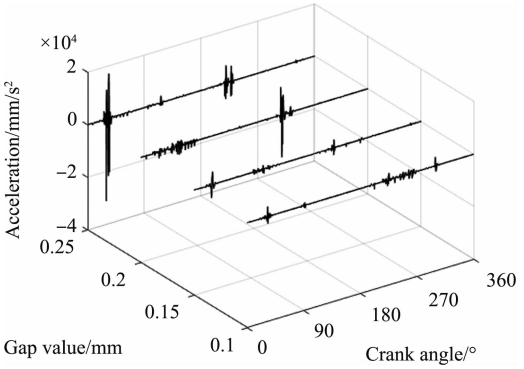

(b) Vertical direction

Fig. 7 Crosshead acceleration under different clearances

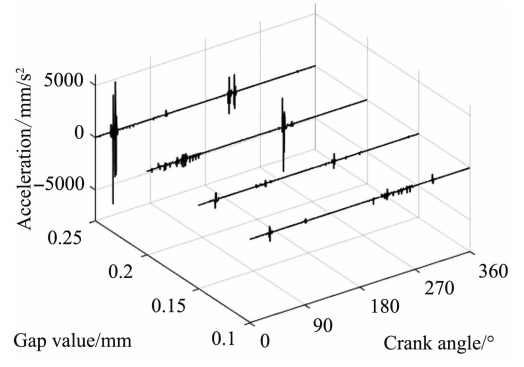

(a) Horizontal direction

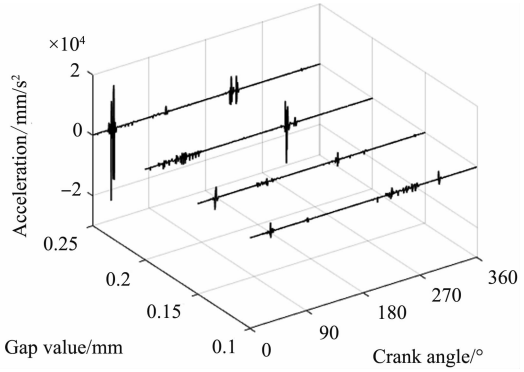

(b) Vertical direction

Fig. 8 Vibration acceleration of the measurement point under different clearances

Fig. 9 shows the axle center trajectories in one cycle with different gaps. It can be seen that regardless of the size of the gap, the axis trajectory is in an '8' shape, and two contact collisions occurred between the cross head pin and the small head tile, and the impact was mainly in the horizontal direction. The contact collision occurs near crankshaft rotation angles of 30° and 220° and lasts for a period of time, which is consistent with the characteristic parameter impact phenomenon described above.

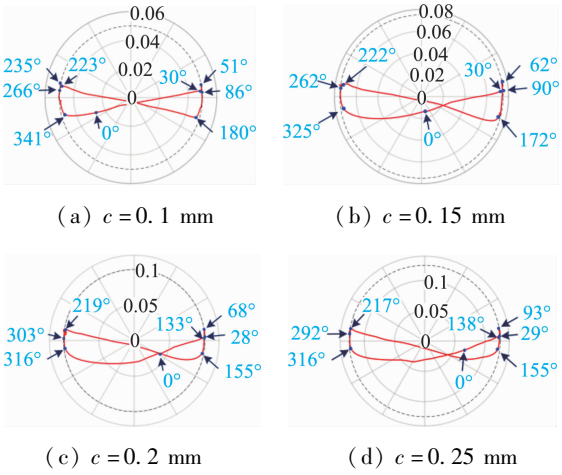

(a) $c = 0.1$ mm (b) $c = 0.15$ mm

(c) $c = 0.2$ mm (d) $c = 0.25$ mm

Fig. 9 Axle center trajectory under different clearances

To check the oil film characteristics at the contact collision phase point, the pressure distribution mesh on the inner surface of the bearing is exported here, as shown in Fig. 10. The surface pressure distribution includes oil film pressure and contact pressure. The origin of the circumferential coordinate in the figure is the intersection of the negative semi-axis of the bearing Y-axis (vertical direction) and the contour, and the positive direction is the clockwise direction. When the crankshaft angle is 34°, the surface pressure is the largest at the position of 270° in the circumferential direction, and the pressure is mainly the contact pressure component. When the crankshaft angle is 226°, the surface pressure at the position of 90° in the circumferential direction is the largest, and the pressure is mainly the contact pressure. At the beginning of the contact collision (that is, the crankshaft angle of 30° and 220°), both the contact pressure and the oil film pressure are extremely unstable, the motion state between the pin and holes changes from lubrication to contact, and the oil film pressure and contact pressure both have sudden changes and sharp angles, and the system presents instability and chaos. As the collision energy is dissipated and the system is stabilized, the mixed lubrication is gradually dominated by the contact, and the surface pressure is mainly represented by the contact pressure. It can be found that the contact pressure presents an axial distribution, and the contact pressure is mainly distributed at both ends.

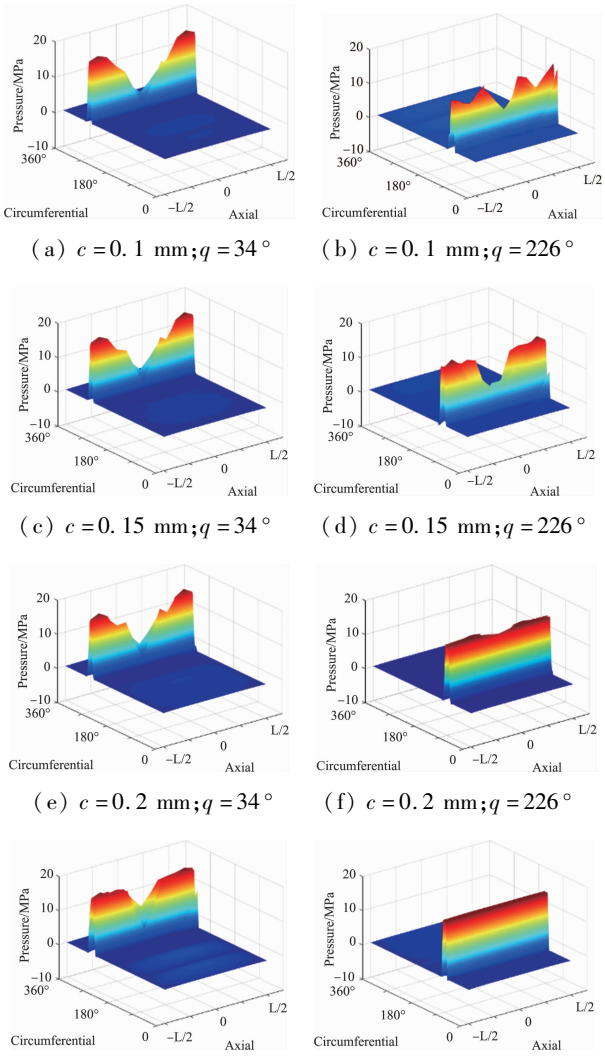

(a) $c = 0.1$ mm; $q = 34°$ (b) $c = 0.1$ mm; $q = 226°$

(c) $c = 0.15$ mm; $q = 34°$ (d) $c = 0.15$ mm; $q = 226°$

(e) $c = 0.2$ mm; $q = 34°$ (f) $c = 0.2$ mm; $q = 226°$

(g) $c = 0.25$ mm; $q = 34°$ (h) $c = 0.25$ mm; $q = 226°$

Fig. 10 Schematic diagram of surface pressure distribution

3.2 Influence of variable clearance at different speeds

To study the effect of the clearance on the dynamic behavior of the mechanism at different speeds, two other speeds (300 r/min and 375 r/min) are set here. From subsection 3.1, it can be seen that the impact amplitude and phase of different dynamic responses under the same working condition are corresponding. Here, the bearing reaction force is extracted to explore the fault response law at different speeds. Fig. 11 shows the bearing reaction curves at different speeds at a clearance of 0.1 mm. From the phase point of view, with the increase of the rotational speed under the same clearance, the phase of the contact impact is advanced, and the commutation point of the bearing reac-

tion force is also advanced. Define the first collision impact between the pin and the bearing in one cycle as Impact 1, and the collision impact between the pin and the inner wall of the other side of the bearing as Impact 2. The time domain ranges of Impact 1 and Impact 2 under different conditions are defined in Table 3, whose data in the table are the average of ten cycles. And it can be found that the above phase change law is universal.

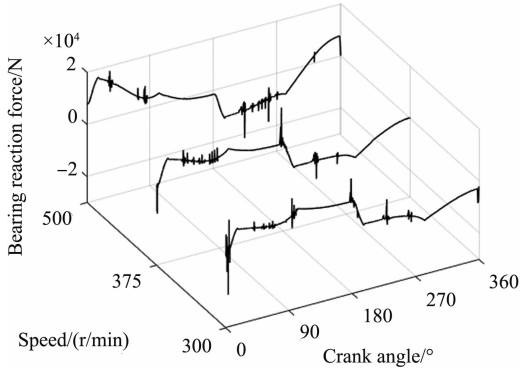

Fig. 11 Bearing reaction force at different speeds

Fig. 12 illustrates the variation pattern of the peak value of Impact 1 and Impact 2 with speed for the four gaps. The peak value of the impact is obtained by averaging the data over ten cycles. From the perspective of the impact amplitude, with the increase of the rotational speed, the impact amplitude of the bearing reaction force under normal conditions is almost unchanged; but in the wear condition, with the increase of the rotational speed, the impact amplitude changes significantly. It can be seen that the vibration response under the wear fault is more sensitive to the change of rotational speed. As the speed increases, the shock peak appears to decrease and then increase, which means that there may be a speed at which the gas and reciprocating inertial forces are balanced to a greater extent.

3.3 Influence of variable clearance under different loads

To further analyze how the wear condition affects the dynamic response under variable load conditions, five groups of gas loads of 30%, 50%, 70%, 90% and 100% were set. Fig. 13 shows the bearing reaction force curves of variable loads under normal and c = 0.15 mm conditions at a speed of 500 r/min. For the same clearance, with the change of load, the commutation points of the bearing reaction force change, and the number of commutation changes under low load conditions. At the same time, the new commutation point will bring new shocks, as shown in the circle in Fig. 13(b). The phase range of the collision impact under variable load is shown in Table 3. It can be seen that when the adjustment method of this paper is used, the phase of the start of the shock basically does not change

Table 3 The phase distribution of Impact1 and Impact 2 for different conditions

unit: °

load	gap	300 r/min	375 r/min	500 r/min
rpm				
30%	0.1 mm	39-92 225-288	38-90 224-259	32-112 219-257
	0.15 mm	41-144 231-313	38-79 225-271	29-52 223-262
	0.2 mm	48-80 230-243	46-50 227-257	27-48 218-267
	0.25 mm	40-75 226-256	36-72 224-242	27-65 216-265
50%	0.1 mm	39-90 228-275	38-86 224-272	32-119 222-289
	0.15 mm	42-110 232-303	39-129 227-297	29-80 220-262
	0.2 mm	41-62 227-232	28-73 225-230	27-62 218-274
	0.25 mm	40-74 227-257	34-84 222-241	28-61 215-288
70%	0.1 mm	39-84 228-268	36-90 225-267	32-86 218-320
	0.15 mm	41-111 231-281	39-101 222-265	30-74 221-261
	0.2 mm	41-65 234-247	36-45 224-245	29-53 219-247
	0.25 mm	40-54 233-236	36-103 224-295	27-111 218-252
90%	0.1 mm	40-85 229-266	38-90 224-265	32-84 222-321
	0.15 mm	42-116 231-273	38-113 223-267	29-81 219-237
	0.2 mm	41-65 231-247	37-44 222-257	28-75 219-263
	0.25 mm	39-87 231-241	37-99 226-274	25-110 217-252
100%	0.1 mm	40-82 228-267	38-84 227-261	30-85 217-322
	0.15 mm	41-134 229-257	38-119 223-275	31-95 222-244
	0.2 mm	40-79 230-241	38-70 223-248	28-100 220-276
	0.25 mm	39-76 228-246	35-106 227-290	26-112 216-253

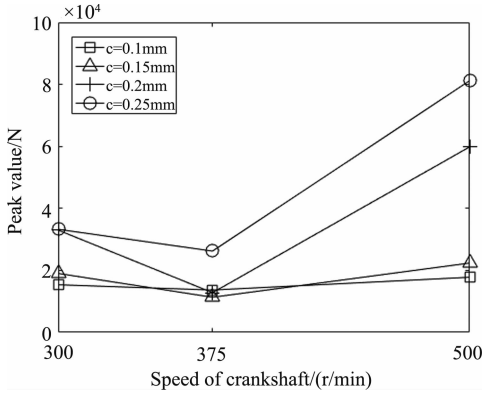

(a) Peak value of Impact 1

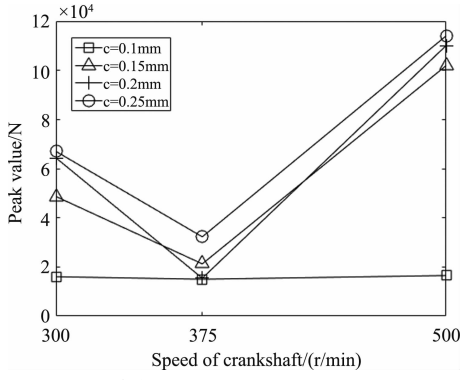

(b) Peak value of Impact 2

Fig. 12 Peak value of impact at different speeds

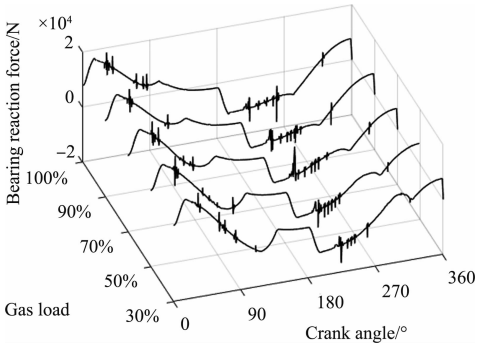

(a) $c = 0.1$ mm

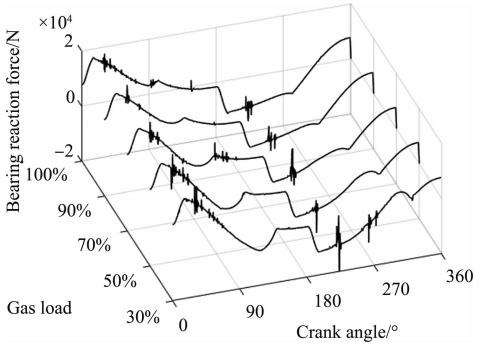

(b) $c = 0.15$ mm

Fig. 13 Bearing reaction at different speeds under normal and fault conditions

for different loads, while the duration of the shock changes. Fig. 14 illustrates the variation pattern of the peak value of Impact 1 and Impact 2 with gas loads for the four gaps. The peak value is obtained by averaging the data from 10 simulation cycles. It can be found that as the load increases, the overall impact peak has a rising trend, and the larger the gap value, the greater the fluctuation of the peak value with the change of load.

Fig. 15 shows the minimum oil film thickness curves of different loads. Under normal clearance, with the change of load, the variation law of the minimum oil film thickness in a cycle is basically the same. However, under fault gap, as the load decreases, the minimum oil film thickness at low load jumps in some phases, which corresponds to the phase of the new commutation point that appears at low load in Fig. 13(b). This is because the reverse bearing reaction force temporarily disengages the crosshead pin from the surface of the bearing, as shown in Fig. 15(b) axis trajectory diagram. Therefore, under the wear fault, the oil film characteristic parameters are more sensitive to the change of the gas load, and the minimum oil film thickness and the axis trajectory show more fluctuations with the increase of the bearing reaction force commutation frequency.

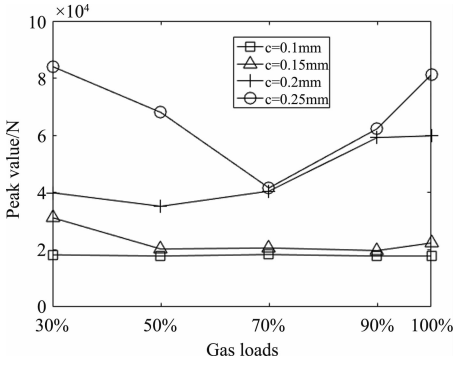

(a) Peak value of Impact 1

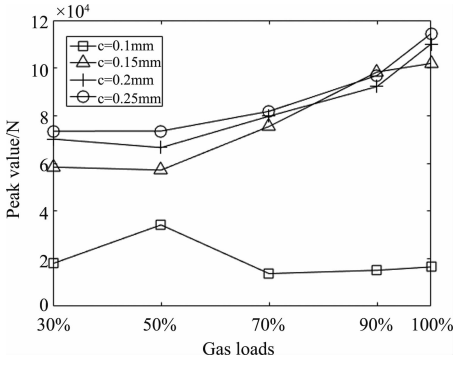

(b) Peak value of Impact 2

Fig. 14 Peak value of impact at different gas loads

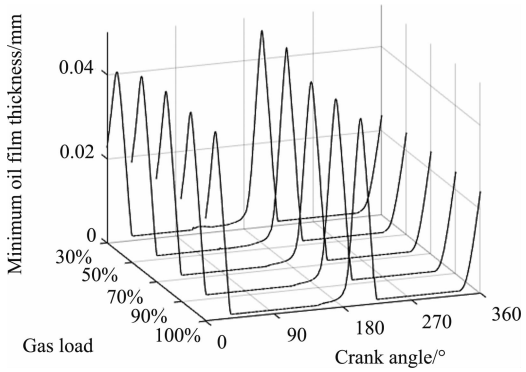

(a) c = 0.1 mm

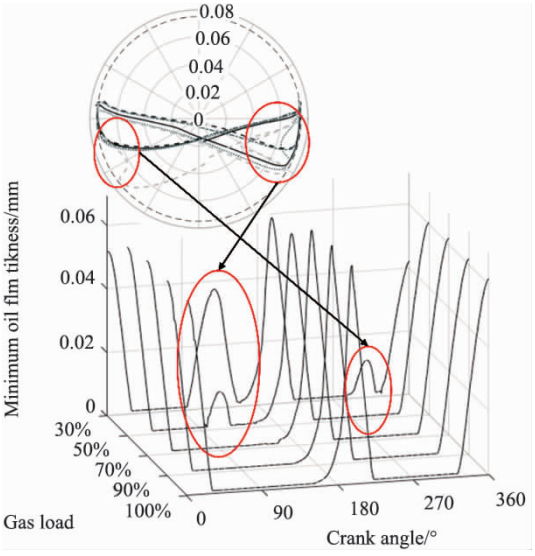

(b) c = 0.15 mm

Fig. 15 Minimum oil film thickness under different loads

4 Conclusions

(1) The crosshead pin's axle center trajectory has a figure of '8' shape; the connecting rod bearing will have two collisions in one cycle, and the collision impact occurs near the crankshaft angle of 30° and 220°; the surface pressure at the point of impact is dominated by contact pressure; the impact mainly occurs in the horizontal direction (X-direction), and the vibration transmission direction is also mainly in the horizontal direction, so the bearing reaction force, the main component direction of eigenvalues such as crosshead acceleration is the horizontal direction, and the vibration amplitude is about 10 times that of the vertical direction. Due to the relative position, the mid-body slide surface measurement points better retain the vertical direction vibration.

(2) From the amplitude of the impact: when the wear fault occurs, the impact caused by the collision is more severe, for example, the vibration amplitude of the surface monitoring point is about 2 – 7 times the normal condition for different fault gaps. The dynamic response of the bearing is more sensitive to the rotational speed under wear conditions, and the impact amplitude will change significantly with the increase of rotational speed compared with the normal clearance. Under the wear condition, the impact amplitude tends to rise with the increase of load, and the amplitude fluctuates sharply with the change of load under the large gap condition.

(3) From the perspective of the phase of the impact: as the speed increases, the phase of the impact will advance, for example, compared to the speed of 300 r/min, the phase of the shock at 500 r/min is advanced by about 10°. This is because as the rotational speed increases, the increase of the reciprocating inertia force changes the reaction force at the bearing, the commutation point of the acting force is advanced, and the impact phase is advanced accordingly. The load affects the duration of the shock but does not change the phase at which the shock starts, which can also be explained in the diagram of the bearing reaction force. This conclusion provides ideas for the location of the angular domain signal segment and its in-depth analysis in the process of fault signal processing.

(4) From the axle center trajectory, under the wear fault, there is an obvious change in the axle center trajectory under low load conditions, and the thickness of the minimum oil film appears to jump significantly at the bearing reaction force commutation point. This is because the change of the gas force leads to the change of the bearing reaction force, the phase and number of the commutation points change, and the movement state of the crosshead pin changes accordingly.

References

[1] SONG B K. Experimental study and numerical simulation of film thickness to the mixed lubrication in point contacts [D]. Beijing: Tsinghua University, 2004: 1-16 (In Chinese).

[2] LIU J F. Failure analysis and improvement measures for connecting rod burning shell on reciprocating compressor [J]. Compressor Technology, 2015(5): 62-64.

[3] FLORES P. Modeling and simulation of wear in revolute clearance joints in multibody systems [J]. Mechanism and Machine Theory, 2009, 44(6): 1211-1222.

[4] DANIEL G B, CAVALCA K L. Analysis of the dynamics of a slider-crank mechanism with hydrodynamic lubrication in the connecting rod-slider joint clearance [J]. Mechanism and Machine Theory, 2011, 46(10): 1434-1452.

[5] PATIR N, CHENG H S. An average flow model for determining effects of three-dimensional roughness on partial hydrodynamic lubrication [J]. Journal of Tribology, 1979, 100: 12-17.

[6] GREENWOOD J A, TRIPP J H. The contact of two nomi-

nally flat rough surfaces[J]. Proceedings of the Institution of Mechanical Engineers, 1970, 185:625-634.
[7] ZHAO B, ZHANG Z N, FANG C C, et al. Modeling and analysis of planar multibody system with mixed lubricated revolute joint[J]. Tribology International, 2016, 98:229-241.
[8] ZHAO B, ZHOU K, XIE Y B. A new numerical method for planar multibody system with mixed lubricated revolute joint[J]. International Journal of Mechanical Sciences, 2016, 113:105-119.
[9] WANG Z, ZHANG J, JIANG Z, et al. A transient and time lag deformation alternating-coupling micro elastohydrodynamic lubrication model[J]. International Journal of Mechanical Sciences, 2021, 210(15):106744.
[10] CHEN X, WANG T, JIANG S. Study on dynamic behavior of planar multibody system with multiple lubrication clearance joints[J]. European Journal of Mechanics-A/Solids, 2021(10):104404.
[11] MACHADO T H, CAVALCA K L. Modeling of hydrodynamic bearing wear in rotor-bearing systems[J]. Mechanics Research Communications, 2015, 69:15-23.
[12] ALVES D S, FIEUX G, MACHADO T H, et al. A parametric model to identify hydrodynamic bearing wear at a single rotating speed[J]. Tribology International, 2021, 153:106640.
[13] JIANG Z N, MA Z T, ZHOU C, et al. Dynamic analysis of reciprocating compressor transmission mechanism with joint clearance under variable working conditions[J]. Fluid Machinery, 2018, 46(3):6.
[14] LI Y. Research on fault diagnosis for sliding bearing clearance of reciprocating compressor with compound faults[D]. Daqing: Northeast Petroleum University, 2019:24-45 (In Chinese).
[15] XIAO S G. Research on dynamic characteristics of gap wear of reciprocating compressor transmission mechanism[D]. Shanghai: Shanghai University, 2019:53-181 (In Chinese).
[16] DANIEL G B, CAVALCA K L. Analysis of the dynamics of a slider-crank mechanism with hydrodynamic lubrication in the connecting rod – slider joint clearance[J]. Mechanism and Machine Theory, 2011, 46(10):1434-1452.
[17] WANG Y. Research on the principle and optimization method of stepless flow control for reciprocating compressor and its application[D]. Beijing: Beijing University of Chemical Technology, 2019:38-66 (In Chinese).

ZHANG Jinjie, born in 1987. He received his Ph. D degree from Beijing University of Chemical Technology. He is currently working in the School of Mechanical and Electrical Engineering, Beijing University of Chemical Technology. His main research directions are mechanical equipment health management, intelligent diagnosis, big data analysis, compressor energy-saving key technologies.